Published in final edited form as:
Analyst. 2008 December ; 133(12): 1767–1775. doi:10.1039/b802113a.

Differences in magnetically induced motion of diamagnetic, paramagnetic, and superparamagnetic microparticles detected by Cell Tracking Velocimetry

Xiaoxia Jin[a,b], **Yang Zhao**[a], **Aaron Richardson**[a], **Lee Moore**[b], **P. Stephen Williams**[b], **Maciej Zborowski**[*,b], and **Jeffrey J. Chalmers**[*,a]

[a]Department of Chemical and Biomolecular Engineering, The Ohio State University, 140 W 19th Ave, Columbus, OH 43210, USA

[b]Department of Biomedical Engineering, Cleveland Clinic, 9500 Euclid Ave, Cleveland, OH 44195, USA

Abstract

Magnetic separation in biomedical applications is based on differential magnetophoretic mobility (MM) of microparticulate matter in viscous media. Typically, the difference in MM is obtained by selectively labeling the target cells with superparamagnetic iron oxide nanoparticles(SPIONs). We have measured the MM of monodisperse, polystyrene microspheres (PSMs), with and without attached SPIONs as a model of cell motion induced by nanoparticle magnetization, using variable *H* field and Cell Tracking Velocimetry (CTV). As a model of paramagnetic microparticle motion, the MM measurements were performed on the same PSMs in paramagnetic gadolinium solutions, and on spores of a prokaryotic organism, *Bacillus globigii* (shown to contain paramagnetic manganese). The CTV analysis was sensitive to the type of the microparticle magnetization, producing a value of MM independent of the applied *H* field for the paramagnetic species, and a decreasing MM value with an increasing field for superparamagnetic species, as predicted from theory. The SPION-labeled PSMs exhibited a saturation magnetization above $H \cong 64{,}000$ A m^{-1} (or 0.08 tesla). Based on those data, the average saturation magnetizations of the SPIONs was calculated and shown to vary between different commercial sources. The results demonstrate sensitivity of the CTV analysis to different magnetization mechanisms of the microparticles.

INTRODUCTION

Immuomagnetic cell separation has been widely used in separating a large variety of cell types.[1–3] It relies on selective attachment of magnetizable nano- or micro-sized particles to cells to produce a difference in magnetic susceptibility between different cell subsets.[4–9] Further improvement in the performance of magnetic cell separation process depends on the development of highly specific and sensitive magnetic labels and efficient, high-throughput magnetic cell separators. Therefore, characterization of the magnetic particles themselves and the cell/magnetic label particle complex plays an important role in the evaluation and subsequent improvement in the performance of magnetic cell separation systems.

Magnetophoretic mobility (MM) is a parameter used to measure the response of microparticulate matter suspended in a viscous fluid to the applied magnetic field.[10] A cell

Fax: (614) 292-3769; Tel: (614) 292-2727; Chalmers.1@osu.edu. Fax: (216) 444-9198; Tel: (216) 445-9330; Zborowm@ccf.org.

labeled with magnetic nanoparticles acquires a MM that is quantitatively related to the physio-chemical properties of the cell-label complex and the suspending fluid, such as the magnetic susceptibility of the nanoparticles, the hydrodynamic diameter of the cell-label complex, the antibody binding capacity of the cell, and the viscosity of the fluid medium.11 The MM distribution in the cell population depends on the selectivity and specificity of the targeting antibodies and the cell surface antigen expression.[12,13]

To experimentally measure the MM of single, micron-sized particles and cells, we have developed an experimental instrument, referred to as Cell Tracking Velocimetry (CTV).[14, 15] Compared to other methods, such as Gouy and Faraday balances and a superconducting quantum interference device, SQUID, that produce bulk averages,[16,17] CTV measures the magnetic property of a single microparticle or a cell. The magnetically induced velocity, u_m of a cell in a constant magnetostatic field energy gradient, S_m, is measured using microscope and computer tracking velocimetry software on a large set of cells, typically numbering a few thousands.[18] Such analyses allow further improvements in both labels, labeling methodology, and cell separation instrument design and operation.[2,19,20]

In principle, the magnetic properties of materials, whether they are diamagnetic, paramagnetic, ferromagnetic, or superparamagnetic, introduce different functional dependence of MM on the applied field. In particular, the MM of particulate matter suspended in a continuous, viscous medium is directly proportional to the difference of magnetic susceptibilities between the suspended and the suspending phases, $\chi_p - \chi_f$ (particle and fluid, respectively, discussed in the next section). Therefore, the experimentally detected changes of the particle mobility with the applied field correspond to the particle (and fluid) susceptibility changes with the field. For the types of fluids used for cell separation (aqueous solutions of Na^+, Cl^-, phosphates, amino acids, glucose, and proteins, such as 5% w/v bovine serum albumin) the solution is diamagnetic, and therefore, the magnetic susceptibility of the liquid phase is independent of the applied field. The susceptibility of the cell-label complex, however, is largely determined by the susceptibility of the magnetic label, because the cell susceptibility is small by comparison. Typically, the microparticle magnetization saturates in the applied field and therefore, the magnetic susceptibility of the cell-label complex becomes a function of the applied field.

The high sensitivity of the CTV apparatus to the motion of single microparticles in response to the applied magnetic field, and its ability to measure mobility distribution on large sets of microparticles, allowed us to compare the functional dependence of MM on the applied field for different types of magnetic microparticles. As a model of the saturated magnetization microparticle, we have selected monodisperse, polystyrene microspheres (PSMs) complexated with dextran nanoparticles doped with magnetite. As a model of the unsaturated magnetization (paramagnetic) microparticles, the spores of a bacterium containing paramagnetic manganese, *Bacillus globigii*, were selected. Also, the effect of a paramagnetic gadolinium solution on the mobility of unlabeled (diamagnetic) PSMs was investigated. In this study, the two different magnetic responses of the viscous suspensions of the particulate matter to varying magnetic fields are presented and discussed by using the latest version of the CTV that incorporates control over the (variable) applied magnetic field.

THEORY

Magnetophoretic mobility

Magnetophoretic mobility, m, has been previously defined[10] as the magnetically induced velocity, u_m, divided by the local magnetostatic energy gradient, S_m:

$$m = \frac{u_m}{S_m} \tag{1}$$

For particle motion in one dimension, applicable to the CTV magnetic field design, the parameter S_m becomes:

$$S_m \equiv \frac{d}{dx}\left(\frac{B_0^2}{2\mu_0}\right) = \frac{1}{2\mu_0}\frac{dB_0^2}{dx} = \frac{1}{2}\mu_0\frac{dH^2}{dx} \tag{2}$$

where $B_0 = \mu_0 H$ is the magnetic field induction (in units of tesla, T), H is the strength of the applied magnetic field (in units of ampere/meter, or A m^{-1}) and μ_0 is the magnetic permeability of a vacuum with a value of $4\pi \times 10^{-7}$ Tm A^{-1} (S.I. units system is used throughout this work).[21] In this paper, the applied field strength H is used interchangeably with the field induction B_0 as the type of the media used for cell separation have negligible effect on the local field induction B.[22]

In the limiting case of a microsphere undergoing creeping flow in viscous media, the MM becomes:

$$m_{\mu s} = \frac{u_m}{S_m} = \frac{\left(\chi_{\mu s} - \chi_f\right) V_{\mu s}}{3\pi D_{\mu s}\eta} = \frac{\Delta\chi D_{\mu s}^2}{18\eta} \tag{3}$$

where $D_{\mu s}$ is the diameter of the microsphere with a magnetic susceptibility of $\chi_{\mu s}$, χ_f is the susceptibility of the fluid, $V_{\mu s}$ is the volume of the microsphere, and η is the viscosity of the fluid.[23]

The MM of the microsphere is directly proportional to the difference of magnetic susceptibilities of the particle and the suspending media, eqn (3). The form of eqn (3) is analogous to that for the particle sedimentation coefficient (with the particle and fluid magnetic susceptibilities, $\chi_{\mu s}$ and $\chi_{\mu f}$, playing the role of the particle and fluid mass densities, $\rho_{\mu s}$ and ρ_f, compare with eqn (10), below). Therefore, it has been occasionally referred to in the literature as the "magnetic Archimedes effect".[24, 25] Consequently, the MM of a particle is a simple function of the material properties of the particle and the suspending media (in particular, their magnetic susceptibilities). When measured experimentally by CTV in media of known susceptibility and viscosity (such as aqueous solutions), MM provides a direct measure of the particle magnetic susceptibility.[23,26,27] Conversely, when CTV is used in combination with calibration particle standards, such as monodisperse PSMs, the MM of such standards provides a direct measure of the unknown fluid magnetic susceptibility.[23] It has been shown recently that the application of MM determination by CTV can be extended to measurements of magnetic properties of the nanoparticles themselves.[26] For the case of the microsphere complexated with the magnetic nanoparticles attached to its surface, the magnetophoretic mobility m of the thus labeled microsphere is expressed by adding a correction m_{ns} to the mobility of the un-labeled microsphere $m_{\mu s}$:

$$\begin{aligned} m &= m_{\mu s} + m_{ns} \\ &= \frac{(\chi_{\mu s} - \chi_f)V_{\mu s}}{3\pi D_t \eta} + \frac{N_{ns}(\chi_{ns} - \chi_f)V_{ns}}{3\pi D_t \eta} \end{aligned} \tag{4}$$

where N_{ns} is the number of magnetic nanoparticles bound to the microsphere, χ_{ns} is the magnetic susceptibility of the nanoparticle with a volume of V_{ns}, and D_t is the equivalent spherical diameter of the microsphere-nanoparticle complex. For the case of a cell labeled with magnetic nanoparticles, the same formula applies with the $m_{\mu s}$ and D_t substituted by the characteristic MM and the hydrodynamic diameter of the labeled cell, respectively.

The dependence of the magnetophoretic mobility on the applied field, *H*

For diamagnetic and paramagnetic particles, whose magnetization, *M*, is directly proportional to the applied field, *H*, the magnetic susceptibility, χ, is independent of the applied field:

$$\chi = \frac{M}{H} \tag{5}$$

The same applies to the diamagnetic and paramagnetic media, and therefore, for such systems, the MM of suspended particles is independent of the applied field, eqns (3) and (4).

However, complications arise in CTV measurements of non-linear magnetic materials for which the ratio of particle magnetization to the applied field in eqn (5) is not constant. The difficulty stems from the fact that the driving force of the magnetically induced velocity is the gradient of the magnetostatic energy density, S_m (eqn (2)), which requires that the field, *H*, changes along the particle trajectory. As the field changes, so does the particle magnetic susceptibility, χ_p. This introduces field-dependent contributions to the expression for the particle MM, eqn (3) which, in principle, could be measured by the CTV.

An important class of non-linear magnetic materials includes the ferromagnetic materials, such as iron oxides, which are typically contained within the nanoparticles used for magnetic cell labeling.[27] Another important class of material used corresponds to the superparamagnetic materials, such as superparamagnetic iron oxide nanoparticles (SPIONs).[28, 29] In this case, the particle size is equal to or smaller than the theoretical size of single domain; thus, there is no domain wall movement upon magnetization. There is no hysteresis, implying, no coercivity or remnant magnetization.[30] However, such particles undergo saturation magnetization at relatively weak fields, much lower than that typically used for CTV analysis (Fig. 1). In order to extend the application of CTV analysis to ferromagnetic and superparamagnetic particles, the expression for MM of such particles has to be reinterpreted by introducing terms characteristic of non-linear magnetic materials, such as the saturation magnetization, M_S. This is accomplished by extending the definition of the magnetic susceptibility, eqn (5), to the magnetically saturated materials.[31] For those materials the magnetic susceptibility becomes inversely proportional to the field, *H* (Fig. 1):

$$\chi = \chi(H) = \frac{M_s}{H} \tag{6}$$

Furthermore, by treating the parameter χ formally, as defined by eqn (6), one may substitute χ in eqn (4) by the RHS of eqn (6) and thus arrive at the expression for the MM of a PSM complexated with superparamagnetic nanoparticles in a saturating, magnetic field, as obtained by Zhang et al.[26]:

$$m = m_{\mu s} + \frac{N_{ns}\left(\frac{\mu_0 M_s}{B_0} - \chi_f\right) V_{ns}}{3\pi D_t \eta} \tag{7}$$

where M_s is the saturation magnetization of the nanoparticles and $B_0 = \mu_0 H$. Note that the suspending fluid (physiologic electrolyte solution in water) and the PSM that binds the magnetic nanoparticles, are diamagnetic and therefore, χ_f and $\chi_{\mu s}$ are independent of the applied field. This equation shows that for saturated SPIONs binding to the PSM, the MM of the PSM-SPION complex decreases with the increasing, applied magnetic field, B_0.

The above analysis shows that the magnetically induced motion of the microparticles depends on the material property of the microparticle. For paramagnetic and diamagnetic particles in paramagnetic or diamagnetic fluid media (linearly polarizable materials, for short), the magnetically induced particle velocity is directly proportional to the gradient of the square of the local magnetic field intensity, dB_0^2/dx. This is shown by combining eqns (1), (2) and (3), from which one obtains:

$$u_m = mS_m = \frac{\Delta\chi D_{\mu s}^2}{36\mu_0\eta}\frac{dB_0^2}{dx}, \quad \Delta\chi = \text{const} \tag{8}$$

In comparison, the presence of the bound superparamagnetic nanoparticles on the surface of the PSMs introduces saturation magnetization effects that weaken the dependence of the PSM velocity on the applied field so that the velocity becomes directly proportional to dB_0/dx. This is shown by combining eqns (1), (2), and (7), and by dropping in eqn (7) terms related to the diamagnetic properties of the microsphere and the suspending fluid ($m_{\mu s}$ and χf) that are small compared to the term related to the superparamagnetic properties of the nanoparticles (M_s):

$$\begin{aligned} u_m = mS_m &\approx \frac{\mu_0 M_s N_{ns} V_{ns}}{6\mu_0\pi\eta D_t B_0}\frac{dB_0^2}{dx} \\ &= \frac{M_s N_{ns} V_{ns}}{3\pi\eta D_t}\frac{dB_0}{dx}, \quad M_s = \text{const} \end{aligned} \tag{9}$$

The ratio of particle magnetically-induced particle velocity, u_m, to its sedimentation velocity, u_g

The direction of the magnetic field gradient in the CTV apparatus is along x and orthogonal to the direction of the gravity (see Fig. 2(a)). Typically, the magnetically-induced velocity is on the order of magnitude of the particle sedimentation velocity, u_g. This provides an opportunity to normalize the particle magnetophoresis by the gravitational settling effects and eliminate parameters related to viscous drag, η and $D_{\mu s}$. The particle sedimentation coefficient, s, is defined as:

$$S = \frac{u_g}{g} = \frac{\left(\rho_{\mu s} - \rho_f\right) V_{\mu s}}{3\pi D_{\mu s}\eta} = \frac{\Delta\rho D_{\mu s}^2}{18\eta} \tag{10}$$

where $g = 9.81\ \text{m s}^{-2}$ is the standard gravitational acceleration. The formal resemblance of the expression for s to that of the magnetophoretic mobility, m (eqn (3)) was already noted, above.

Linearly polarizable magnetic materials, Δχ = const

Dividing eqn (3) by eqn (10), one eliminates η and $D_{\mu s}$ to obtain:

$$\frac{u_m}{u_g} = \frac{\left(\chi_{\mu s} - \chi_f\right)}{\left(\rho_{\mu s} - \rho_f\right)}\frac{S_m}{g} \tag{11}$$

Eqn (11) can be further rearranged so that:

$$\frac{u_m}{u_g}\frac{g\Delta\rho}{S_m}=\chi_{\mu s}-\chi_f \tag{12}$$

Therefore, a plot of $u_m g\Delta\rho/u_g S_m$ as a function of χ_f is expected to provide a straight line in which the *y*-intercept is the magnetic susceptibility of the microsphere.

Magnetically saturated materials, M_s = const

Dividing eqn (9) by eqn (10), in which $D_{\mu s}$ is substituted by D_t one arrives at:

$$\frac{u_m}{u_g}=\frac{6M_sN_{ns}V_{ns}}{\pi\Delta\rho D_t^3 g}\frac{dB_0}{dx}=\frac{M_{s,ave}}{\Delta\rho g}\frac{dB_0}{dx} \tag{13}$$

where $M_{s,ave}$ is the weighed average saturation magnetization of the PSM complexated with superparamagnetic nanoparticles, which has a total volume of V_t:

$$N_{s,ave}=M_s\frac{N_{ns}V_{ns}}{V_t}=\frac{6M_sN_{ns}V_{ns}}{\pi D_t^3} \tag{14}$$

Here, a plot of u_m/u_g against dB_0/dx is expected to produce a straight line. By measuring the ratio of the magnetically induced velocity and the settling velocity at different values of the magnetic field gradient, and reducing the data to the plot of u_m/u_g as a function of dB_0/dx, one obtains the saturation magnetization of the labeled microsphere complex, $M_{s,ave}$ from the slope.

In summary, the theoretical analysis of the particle magnetophoresis in a well defined magnetic field leads to quantitative predictions of material properties of the particle (its magnetic susceptibility and density) and the effect of superparamagnetic nanoparticle binding (average saturation magnetization of the microsphere-nanoparticle complex). In this study, these predictions are tested by using the latest version of the CTV system in which the permanent magnet assembly has been replaced with electromagnets allowing control over the magnetophoretic driving force, S_m.

MATERIALS AND METHODS

Variable-field version of CTV

To increase the capability of CTV to analyze magnetic particles and cells over a range of magnetic energy gradients, S_m, the permanent magnet assembly was replaced with an electromagnetic system, Fig. 2(a). The electromagnet was designed to have a magnetic energy gradient that could range from zero to a maximum of 106 TA mm^{-2}, approximately equivalent to the previously described permanent magnet, CTV system.[15] These electromagnets were then placed in the previously designed CTV magnetic circuit such that the interpolar gap which produced the magnetic energy gradient was unchanged. The current to the coils is supplied by a programmable DC power supply (Model HPD 60–5, Xantrex, Vancouver, British Columbia). It is operated in a constant current mode and has a range of 0 to 5 A. In the constant current mode, an internal feedback control loop adjusts the voltage to keep a constant current if the resistance of the coils changes. The power supply is interfaced with the computer using a GPIB connection. It is controlled using the CTV software. The dependence of the magnetic field

B_0 and the magnetic energy density gradient, S_m, on the electric current, I, at the center of the microscope's field of view is shown in Fig. 3.

The microparticle suspension to be analyzed is pumped into a rectangular borosilicate glass channel which is placed in the interpolar gap of the electromagnet as shown in Fig. 2 (a). The microparticle motion analysis is performed in the stationary fluid (no convective flow) after two valves located at the ends of the channel are closed. The motion of microparticles induced by gravity or magnetic force in the region of interest (ROI) is recorded using an inverted microscope and a 30Hz Cohu CCD 4915 camera (Cohu Electronics, San Diego, CA). The captured images are processed by CTV software, which produces an Excel™ (Microsoft Corp., Redmond, WA) file with microparticle positions for 20 equal time intervals, used to calculate microparticle velocity and sample statistics. A computer screen image after the CTV program has tracked particle settling trajectories (in the vertical direction) and the trajectories for the same particles after the magnetic field was switched on (in the horizontal direction) is shown in Fig. 2(b). Additional details of the hardware and software components of the CTV system are described in the Supporting Information.

Solution susceptibility modifiers

The magnetic susceptibility of the suspending fluid was adjusted with a chelating agent and paramagnetic ion, gadolinium, Gd^{3+}, which is marketed under the brand name Optimark® (Mallinckrodt Inc, St. Louis, MO).[23] A phosphate buffered 150 mM saline (PBS) solution was used as a reference ($\chi_f \approx -9.05 \times 10^{-6}$).

Linearly polarizable magnetic microparticles – *Bacillus globigii* spores

Melnik et al. recently reported the observation that the spores of at least three strains of *Bacillus: Bacillus atrophaeus* formally *Bacillus globigii*), *Bacillus thuringiensis*, and *Bacillus cereus* demonstrated significant intrinsic magnetic susceptibility.[32] All three strains when sporulated demonstrated significant MM using the CTV system. Energy dispersive spectroscopy confirmed that this magnetic susceptibility is the result of the presence of the paramagnetic element, manganese (Mn). The *B. globigii* spore suspensions were prepared as described in the original article.[32]

Magnetically saturated materials - micro and nanoparticles

Biotinylated PSMs, SPHERO™ Biotin Polystyrene Particles (Catalog number TP-60–5, Lot number v01, Spherotech Inc., Libertyville, IL) were used in this study. The data sheet for the particles provided by the manufacturer reports that the mean size, based on SEM analysis, is 6.7 micron.

Four types of magnetic nano- and micro-particles were used in this study: MACS™ Anti-Biotin Microbeads (Catalog number 120-000-900, Miltenyi Biotec, CA, USA); Captivate™ ferrorfluid streptavidin (Catalog number C-21476, Molecular Probes, Eugene, OR); BD Streptavidin Imag™ particles-DM (Catalog number 551307, BD Pharmigen, CA, USA); and Dynabeads® MyOne™ streptavidin C1 (Catalog number 650.01, Dynal Biotech ASA, Oslo, Norway). The complexation of the PSMs with four nanoparticle preparations was performed by applying the protocol of Zhang et al.[26] A final microsphere concentration of $5 \times 10_5$/ml was used for each CTV analysis.

RESULTS AND DISCUSSION

Comparison of particle settling and magnetically-induced velocities

The particle diameter calculated by the Coulter Counter method (Fig. 4(a)) is based on the difference in particle electrical impedance and that of the suspending media.[33] The particle

diameter can be also calculated from the particle settling velocity measured by CTV (Fig. 4 (b)) providing that the difference between particle density and that of the suspending fluid media is known, eqn (10). First, we have determined the unknown particle density by applying the particle mean diameter from the Coulter Counter analysis and the mean settling velocity from CTV analysis to eqn (10), to obtain a mean density of 1.052 g cm^{-3} for the PSM. This is consistent with the value of 1.05 g cm^{-3} reported by its manufacturer. Second, the mean density of the PSM was used to calculate the PSMs diameter histogram from the bead settling velocity histogram (Fig. 4(a)). The two PSM diameter distribution histograms (from Coulter and CTV analyses) were compared, as shown in Fig. 4(c). The modes of the main peaks coincided, as expected. However, those of the minor peaks did not. This appears to be related to a broader distribution of the CTV data than those based on the Coulter analysis.

The effect of magnetic nanoparticle binding on the settling velocity of the PSM-nanoparticle complex is illustrated by a shift in the apparent PSM diameter measured by the CTV. The same PSM density of 1.052 g cm^{-3} was used to calculate the diameter of the PSM-nanoparticle complex. Fig. 5(a) shows the histograms of the diameter distributions of the PSMs, one unlabeled and the other immunomagnetically labeled with MACS™ anti-Biotin nanoparticles. A pronounced increase in the apparent PSM diameter (from 6.53 ± 1.42 μm to 7.20 ± 0.73 μm) was observed following complexation with the nanoparticle label. The combined effect of the magnetic nanoparticle label binding to the PSM on MM and on the settling velocity was shown in a dot plot, with the apparent particle diameter shown on the horizontal axis and the particle MM on the vertical axis, Fig. 5(b). A clear separation of the two sets of data (unlabeled and labeled PSMs) can be observed, as emphasized by an arrow. This is interpreted as resulting from the high sensitivity of the CTV analysis to changes in the individual particle motion caused by the magnetic nanoparticle binding.

Linearly polarizable magnetic materials, Δχ = const

Magnetophoretic mobility of polystyrene particles in paramagnetic solutions. The theory predicts that the MM of the PSMs is independent of S_m, eqn (3). This was tested in a set of experiments in which unlabeled PSMs were suspended in solutions of paramagnetic gadolinium at three different concentrations: 0.0625, 0.1, and 0.1667 mol L^{-1}, which corresponds to a χ_f of 1.22×10^{-5}, 2.49×10^{-5}, and 4.76×10^{-5}. The values of susceptibility were calculated from relationships reported by Zhang et al.[26] Changes in the fluid magnetic susceptibility, χ_f, cause changes in the difference between the PSM and the fluid magnetic susceptibilities, $\chi_{\mu s} - \chi_f$, and therefore are expected to lead to changes in the observed PSM magnetophoretic mobility (eqn (3)). This was confirmed by the CTV analysis, showing increasing magnitude of the PSM mobility with the increasing Gd concentration in solution, Fig. 6(a). (The negative values of the PSM mobility derive from the higher susceptibility of the fluid medium than that of the PSM, $\chi_{\mu s} < \chi_f$.) The results also show that the PSM mobility was independent of the applied magnetic field, represented by the magnetic energy density gradient, S_m ranging from 10.3 to 106 TA mm^{-2} for each Gd^{3+} concentration, Fig. 6(a), as expected of the linearly polarizable magnetic materials, eqn (3). We have further reduced the data from Fig. 6(a) to a single plot using eqn (12), and added a datum point corresponding to PSM mobility measurement in phosphate buffered saline (PBS, $\chi_f \approx -0.90 \times 10^{-5}$), as shown in Fig. 6(b). Here the data points lie on a straight line, again as expected of the linearly polarizable materials (eqn (12)). The regression analysis confirms a high degree of correlation between $u_m g \Delta\rho / u_g S_m$ and χ_f ($R^2 = 0.996$, $p = 0.0013$, $N = 24$, slope = −0.974 ± 0.035, expected −1). The y-intercept, $\chi_{\mu s}$, is equal to $-0.80 \pm 0.10 \times 10^{-5}$ and is the same (within the experimental error) as that reported by Zhang et al.[26](-0.77×10^{-5}) and others (the magnetic susceptibility of polystyrene is -0.75×10^{-5}, as quoted by CRC Handbook of Chemistry and Physics[34] and -0.82×10^{-5} reported by Watarai et al.35).

Magnetophoretic mobility of B. globigii spores—The *B. globigii* spore suspensions in PBS are an example of paramagnetic species and, therefore, the MM of the spores is also expected to be independent of the applied field energy gradient, S_m (eqn (3)). This was confirmed by CTV analysis, Fig. 7. Note the large magnitude of the spore MM, larger than that measured for PSM suspensions in Gd solutions, Fig. 6(a). This is related to the magnetization of Mn contained in the spores. The positive value of spore MM reflects the fact that here $\chi_p > \chi_f$. A correlation analysis confirmed that the null hypothesis of the spore mobility being independent of the applied field could not be rejected (Spearman rank order correlation coefficient = −0.267, $p = 0.462$, $N = 9$).

Magnetically saturated materials, M_s = const

Magnetically labeled polystyrene microspheres—In contrast to the paramagnetic species, discussed above, MM was found to be a strong function of S_m for the PSM labeled with the commercial, magnetic nano- and micro-particles. Fig. 8(a) is a plot of MM as a function of S_m from 0.06 to 80 TA mm^{-2} for the biotinylated PSM labeled with MACS™ anti-biotin nanoparticles, Captivate™ ferrofluid streptavidin, Dynabeads® MyOne™ streptavidin, and BD™ Streptavidin Imag-DM. Once the PSMs are labeled with superparamagnetic nanoparticles, a highly non-linear dependence of m on S_m is observed, which is consistent with the saturation magnetization effects of the supperparamagnetic compounds bound to the PSMs (eqn (7)). To further underscore this observation, we note that the magnetically-induced velocity, u_m, of the PSMs labeled with superparamagnetic nanoparticles 15 is a linear function of the magnetic field gradient, in the saturating magnetic field (eqn (13)). In order to verify that prediction, we have re-plotted the data from Fig. 8(a) using dB_0/dx as an independent variable, Fig. 8(b). Indeed, the linear relationships were obtained, indicating that the magnetically labeled PSMs exhibit a saturation magnetization above a B_0 value of approximately 0.08 T which corresponds to a dB_0/dx value of approximately 0.008 T mm^{-1}.

By plotting the ratio of magnetically-induced to settling velocity, u_m/u_g, of the particle as a function of dB_0/dx (above the saturation point, $dB_0/dx \approx 0.008$ T mm^{-1}), and finding the slope of the straight line corresponding to the experimental data, one is able to calculate the average saturation magnetization, $M_{s,ave}$, of the PSM-nanoparticle complex, eqn (13). The results are shown in Fig. 8(c) for the four different combinations of PSM-magnetic nanoparticle complexes. Linear relationships were obtained for each combination, as expected for the magnetically saturated beads. Table 1 presents the slope, intercept, and R^2 for each of the four combinations. From these values, the saturation magnetization of the labeled microsphere complex, $M_{s,ave}$, were determined from eqn (13) and are presented in Table 1. Note that the magnetically induced velocity is 5 to 15 times greater than the gravitational sedimentation velocity ($5 < u_m/u_g < 15$). By combining the mean diameter data of the unlabeled and labeled PSM obtained from CTV, the saturation magnetization of the four magnetic nanoparticles were solved from eqn (14) and are presented in Table 2. The error analysis of this approach is presented in Supporting Information.

In summary, the results show that the MM of the PSM microparticle does not depend on the applied field, as expected of the paramagnetic species. Above the saturating field value, the MM of the PSM-SPION complex decreases in inverse proportion to the applied field, as expected of the magnetically saturated species. The agreement with the theory was demonstrated by showing that for particles that do not saturate in the applied field, the magnetically induced velocity is directly proportional to the gradient of the square of the field, dB_0^2/dx, and that for magnetic label nanoparticles that saturate in the applied field, the magnetically induced velocity of the PSM-label complex is directly proportional to the gradient of the magnetic field, dB_0/dx.

CONCLUSIONS

Cell motion analysis using the microscopic technique of cell tracking velocimetry (CTV) is, in principle, sensitive to the local stresses and the body forces acting on the cell. Our previous studies using a constant magnetic field have demonstrated quantitatively an increase of cell velocity following magnetic nanoparticle binding (Chalmers et al.15), increase of PSM velocity with a concurrent increase in magnetic susceptibility of the fluid medium (Moore et al.23; Zhang et al.26), and increase in erythrocyte velocity with conversion of intracellular iron from low-spin to high-spin state (Zborowski et al.36).

However, the use of constant magnetic field precluded us from testing if the CTV analysis is sensitive to the type of the cell magnetization (paramagnetic versus superparamagnetic), in other words, if it is capable of distinguishing between a paramagnetic and superparamagnetic response of a microscopic particle to the applied field. This has now become possible with the introduction of the variable-field CTV equipped with electromagnets and a controlled current power supply. A convenient measure of the microscopic particle response to the applied field is its magnetophoretic mobility (MM), *m*, a quantity that is directly proportional to the difference between magnetic susceptibilities of the particle and the fluid media. Thus, for a microparticle and a fluid medium whose susceptibilities are independent of the applied field (characteristic of paramagnetic and diamagnetic materials) the microparticle MM is independent of the applied field. In comparison, the presence of the superparamagnetic species results in a decrease of microparticle MM with the increasing field. We have verified the predicted behavior of the microparticle MM in the variable magnetic field on a model of linearly polarizable (paramagnetic and diamagnetic) materials using PSMs in Gd solutions and *B. globigii* spores (known to contain paramagnetic Mn) in PBS solution, and on magnetically saturated materials using PSMs complexated with iron oxide nano- and micro-particles. As predicted, the microparticle MM was constant for linearly polarizable media and was an inverse function of the applied field for the magnetically saturated microparticles, in the range of the applied fields. In addition, the quantitative analysis of the microparticle motion by the CTV and the high statistical 100 power afforded by the ability of multi-particle tracking per frame (producing hundreds to thousands of microparticles tracked per sample) allowed us to calculate characteristic magnetic properties of the microparticles, such as the magnetic susceptibility of the PSMs, and the average saturation magnetization of the PSM-nanoparticles complex. The accuracy of the CTV analysis was confirmed by showing that the calculated PSM susceptibility is equal to that reported by others (within experimental error) and that the PSM settling velocity is equal to the Stokes velocity predicted for the same PSM diameter and density.

The extended capabilities of the electromagnet-based CTV analysis to distinguish between the paramagnetic and superparamagnetic properties of a single microparticle or a cell will be further evaluated in future applications to cell biology, in particular, to cell pathologies.

Supplementary Material

Refer to Web version on PubMed Central for supplementary material.

Acknowledgments

We thankfully acknowledge support by NSF (BES-0124897 and EEC-042526) and the NCI (R01 CA97391A1 and RO1 CA62349).

REFERENCES

1. Safarik I, Safarik M. J Chromatogr B 1999;722:33–53.

2. Jing Y, Moore LR, Williams PS, Chalmers JJ, Farag SS, Bolwell BJ, Zborowski M. Biotechnol. Bioeng 2007;96:1139–1154. [PubMed: 17009321]
3. Zborowski, M.; Chalmers, JJ. Magnetic Cell Separation. Elsevier Science; Amsterdam: 2007. p. 454
4. Winoto-Morbach S, Tchikov V, Muller-Ruchholtz W. J. Clin. Lab. Anal 1995;9:42–46. [PubMed: 7722771]
5. Wilhelm C, Gazeau F, Bacri JC. Eur. Biophys. J 2002;31:118–125. [PubMed: 12012115]
6. Han KH, Frazier AB. J. Appl. Phys 2004;96:5797–5802.
7. Hafeli UO, Lobedann MA, Steingroewer J, Moore LR, Riffle JS. J. Magn. Magn. Mater 2005;293:224–239.
8. Hackett SL, Pierre TG. J. Phys: Conference Series 2005;17:181–184.
9. Pamme N. Lab Chip 2007;7:1644–1659. [PubMed: 18030382]
10. Zborowski M, Moore LR, Williams PS, Chalmers JJ. Sep. Sci. Technol 2002;37:3611–3633.
11. McCloskey KE, Chalmers JJ, Zborowski M. Anal. Chem 2003;75:6868–6874. [PubMed: 14670047]
12. McCloskey KE, Chalmers JJ, Zborowski M. Cytometry 2000;40:307–315. [PubMed: 10918281]
13. Leigh DR, Steinert S, Moore LR, Chalmers JJ, Zborowski M. Cytometry A 2005;66:103–108. [PubMed: 15973696]
14. Chalmers JJ, Haam S, Zhao Y, McCloskey KE, Moore LR, Zborowski M, Williams PS. Biotechnol. Bioeng 1999;64:519–526. [PubMed: 10404232]
15. Chalmers JJ, Zhao Y, Nakamura M, Melnik K, Lasky LC, Moore LR, Zborowski M. J. Magn. Magn. Mater 1999;194:231–241.
16. Cullity, BD. Introduction to Magnetic Materials. Addison-Wesley, Reading; Massachusetts: 1972. p. 74-78.
17. Cantor R, Enpuku K, Ryhänen T, Seppä H. IEEE Trans. Appl. Supercond 1993;3:1800–1803.
18. Nakamura M, Zborowski M, Lasky LC, Margel S, Chalmers JJ. Exp. Fluids 2001;30:371–380.
19. Chosy EJ, Nakamura M, Melnik K, Comella K, Lasky LC, Zborowski M, Chalmers JJ. Biotechnol. Bioeng 2003;82:340–351. [PubMed: 12599261]
20. Williams PS, Zborowski M, Chalmers JJ. Anal. Chem 1999;71:3799–3807. [PubMed: 10489528]
21. Becker, R. Electromagnetic Fields and Interactions. Dover Publications, Inc.; New York: 1982. p. 112
22. Furlani EP, Sahoo Y, Ng KC, Wortman JC, Monk TE. Biomed. Microdevices 2007;9:451–463. [PubMed: 17516176]
23. Moore LR, Milliron S, Williams PS, Chalmers JJ, Margel S, Zborowski M. Anal. Chem 2004;76:3899–3907. [PubMed: 15253623]
24. Jones BA, O'Grady K. J. Appl. Phys 2005;97:1–3.
25. Kitazawa K, Ikezoe Y, Uetake H, Hirota N. Physica B: Condensed Matter 2001;294–295:709.
26. Zhang H, Moore LR, Zborowski M, Williams PS, Margel S, Chalmers JJ. Analyst 2005;130:514–527. [PubMed: 15776162]
27. Pankhurst QA, Connolly J, Jones SK, Dobson J. J. Phys. D: Appl. Phys 2003;36:R167–R181.
28. Bean CP, Livingston JD. J. Appl.Phys 1959;30(Suppl):120S–129S.
29. Kantor, AB.; Gibbons, I.; Miltenyi, S.; Schmitz, J. Cell Separation Methods and Applications. Vol. Editon edn.. Recktenwald, D.; Radbruch, A., editors. Marcel Dekker, Inc.; New York: 1998. p. 153-173.
30. Jacubovics, JP. Magnetism and Magnetic Materials. Cambridge University Press; Cambridge: 1994. p. 165
31. Bozorth, RM. Ferromagnetism. D. van Nostrand Company, Inc.; Princeton, NJ: 1968. p. 968
32. Melnik K, Sun J, Fleischman A, Roy S, Zborowski M, Chalmers JJ. Biotechnol. Bioeng 2007;98:186–192. [PubMed: 17335063]
33. Coulter WH. Proc. Natl. Electron. Conf 1956;12:1034.
34. Weast, R.; Astle, MJ. CRC Handbook of Chemistry and Physics. 1979. p. 123-136.
35. Watarai H, Namba M. Anal.Sci 2001;17:1233–1236. [PubMed: 11990604]

36. Zborowski M, Ostera GR, Moore LR, Milliron S, Chalmers JJ, Schechter AN. Biophys. J 2003;84:2638–2645. [PubMed: 12668472]

37. Moore LR, Zborowski M, Nakamura M, McCloskey K, Gura S, Zuberi M, Margel S, Chalmers JJ. J. Biochem. Biophys. Methods 2000;44:115–130. [PubMed: 10889282]

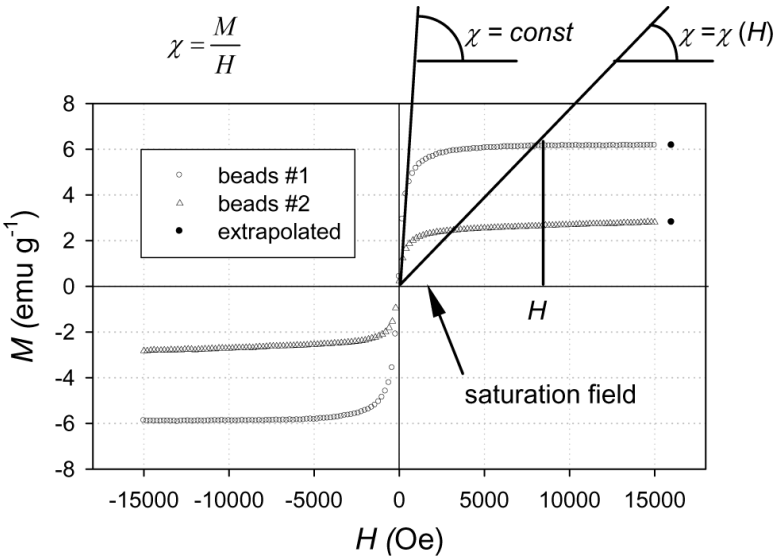

Fig. 1.

Magnetization curves for monodisperse magnetic microspheres (adapted from ref. 37). Measurements were made using Oxford vibrating sample magnetometer. Note the dependence of particle susceptibility on field strength for fields higher than the saturation field. The saturation field is ~1,000 oersted (Oe) in CGS units system. Multiply CGS unit for H (Oe) by $1000/4\pi$ to obtain H (A m^{-1}) in SI unit; and multiply CGS unit for volume magnetization, M (emu cm^{-3}) by 1000 to obtain M (A m^{-1}) in SI unit. Volume magnetization is calculated from the mass magnetization providing that the density of the beads is known.

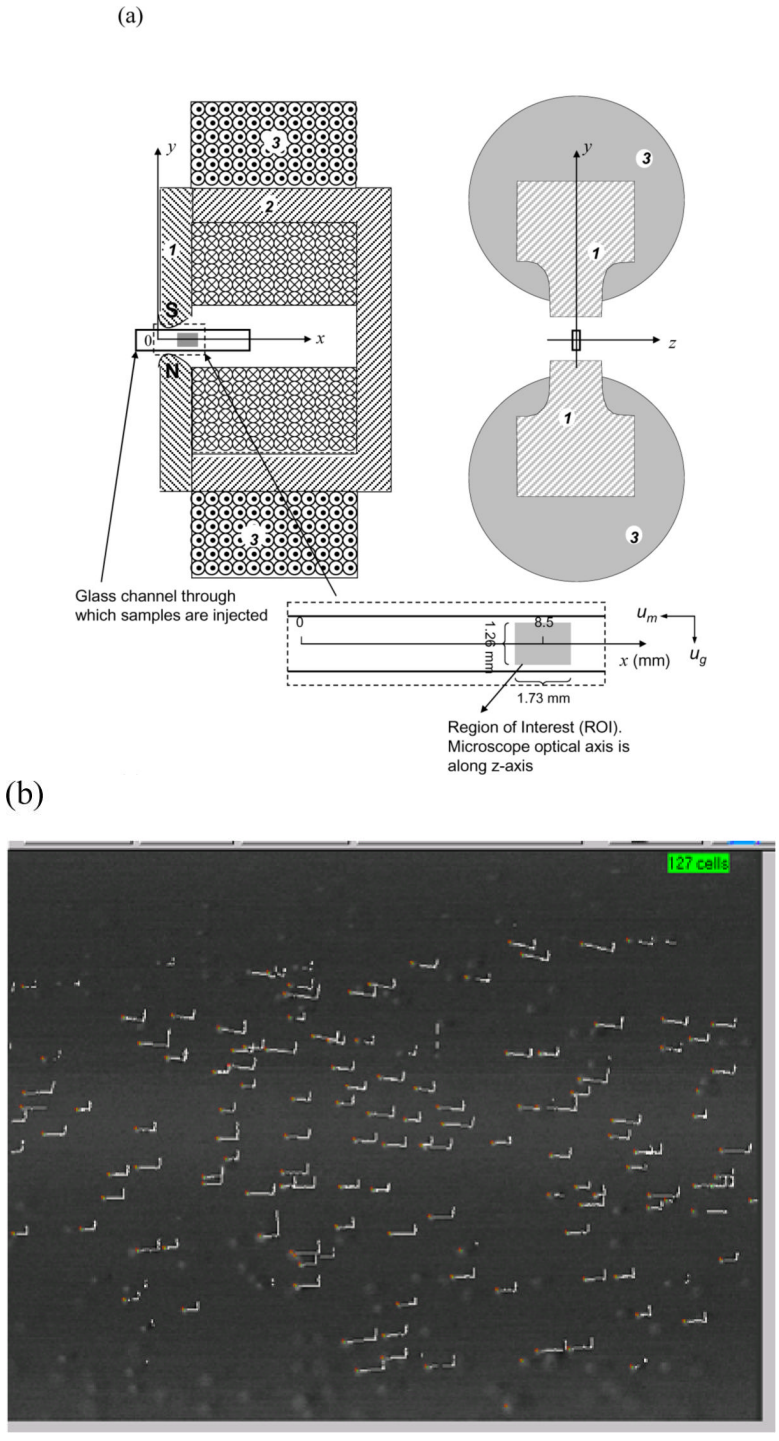

Fig. 2.

(a) Schematic diagram of the relative position of the electric coils and analysis channel for the electromagnetic CTV system. 1, 2 — pole pieces and flux return yolk made of 1018 low-carbon steel; 3 — copper wire coil. (b) Example of the computer screen output of the CTV software indicating settling trajectories (vertical traces) and magnetically induced trajectories (horizontal traces) of particles in ROI tracked by the CTV system.

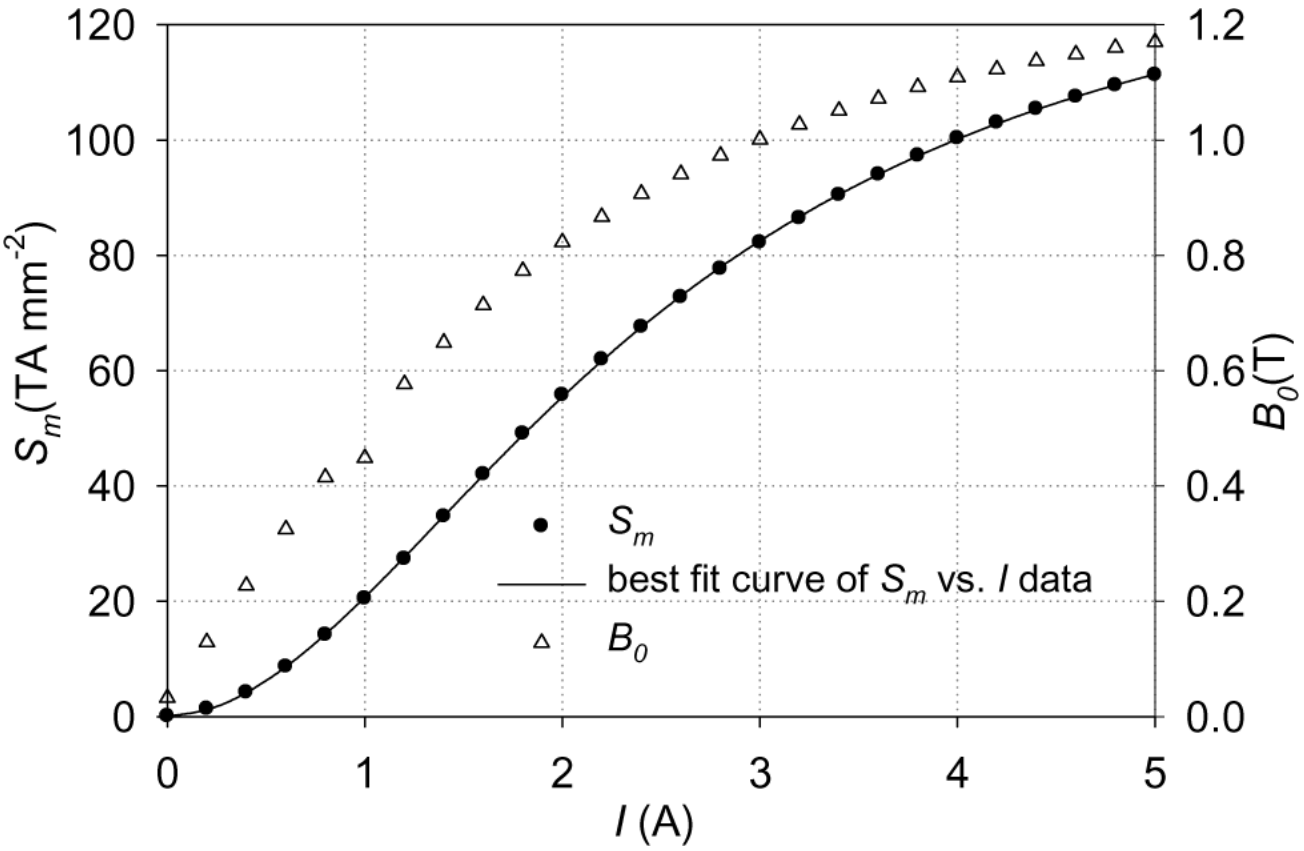

Fig. 3.
Magnetic energy density gradient, S_m, and the applied magnetic field, B_0, as a function of electric current in coils at the center of microscope field of view.

(a)

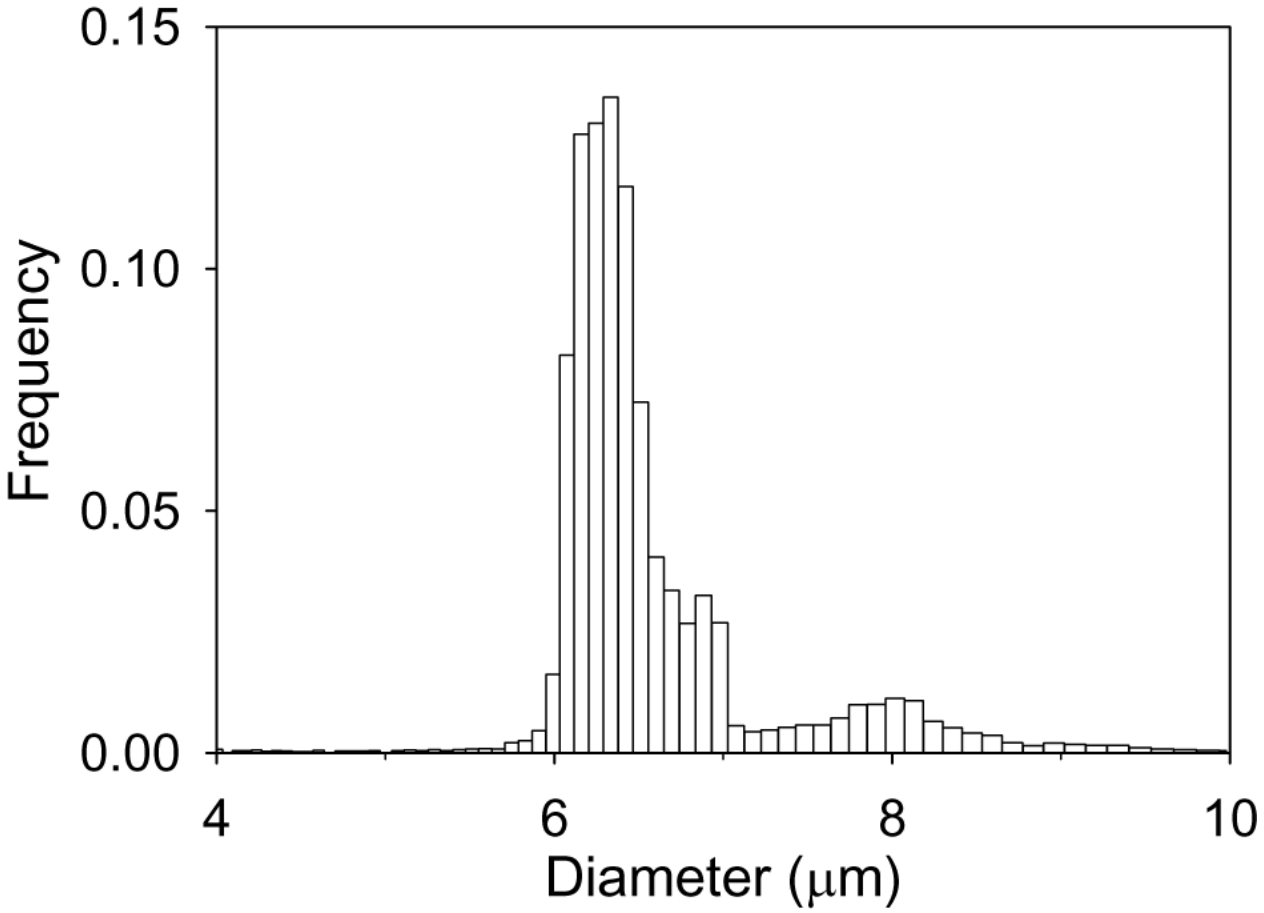

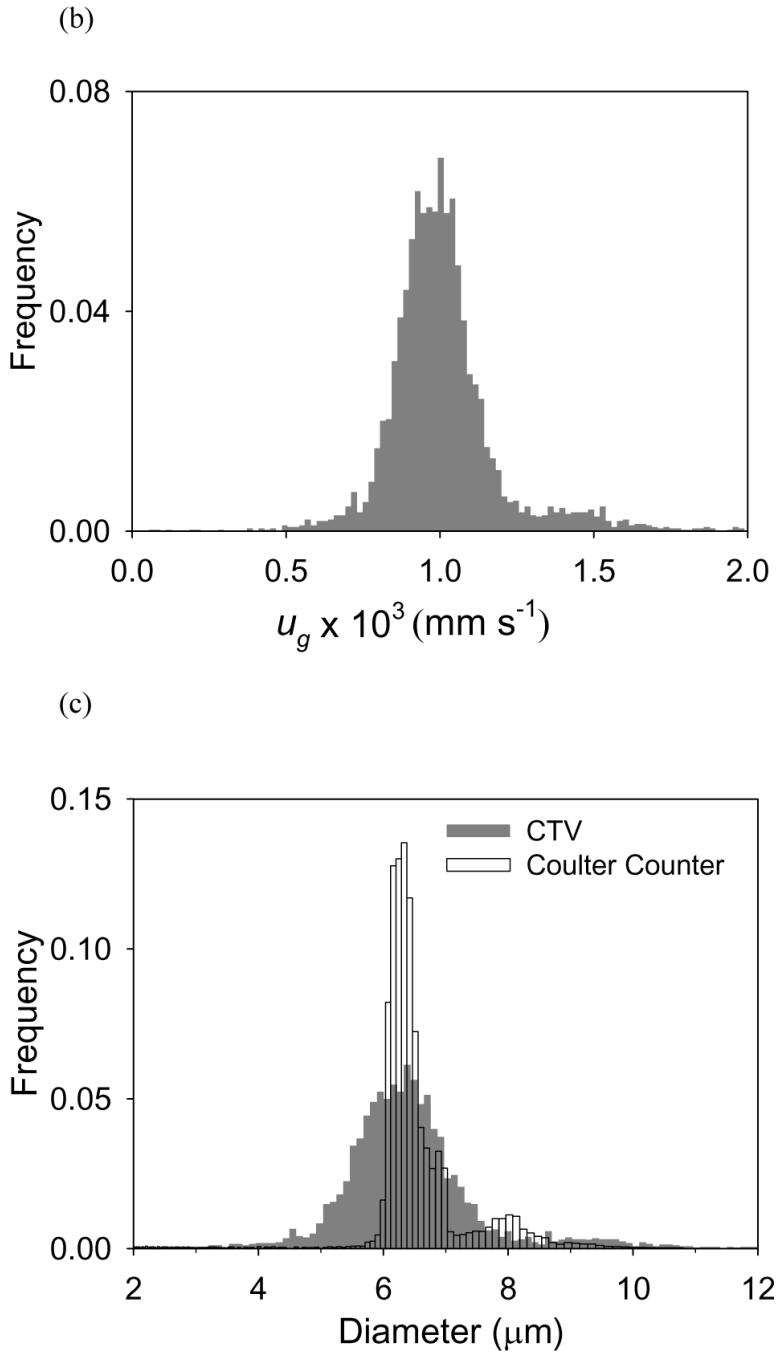

Fig. 4.

(a) Distribution of PSM diameters based on Coulter Counter analysis. (b) The PSM settling velocity, u_g, measured by CTV. (c) Superposition of Coulter Counter histogram and the diameter of the PSMs calculated from CTV settling velocity distribution shown in (b) using an average PSM density of 1.052 g cm^{-3}.

(a)

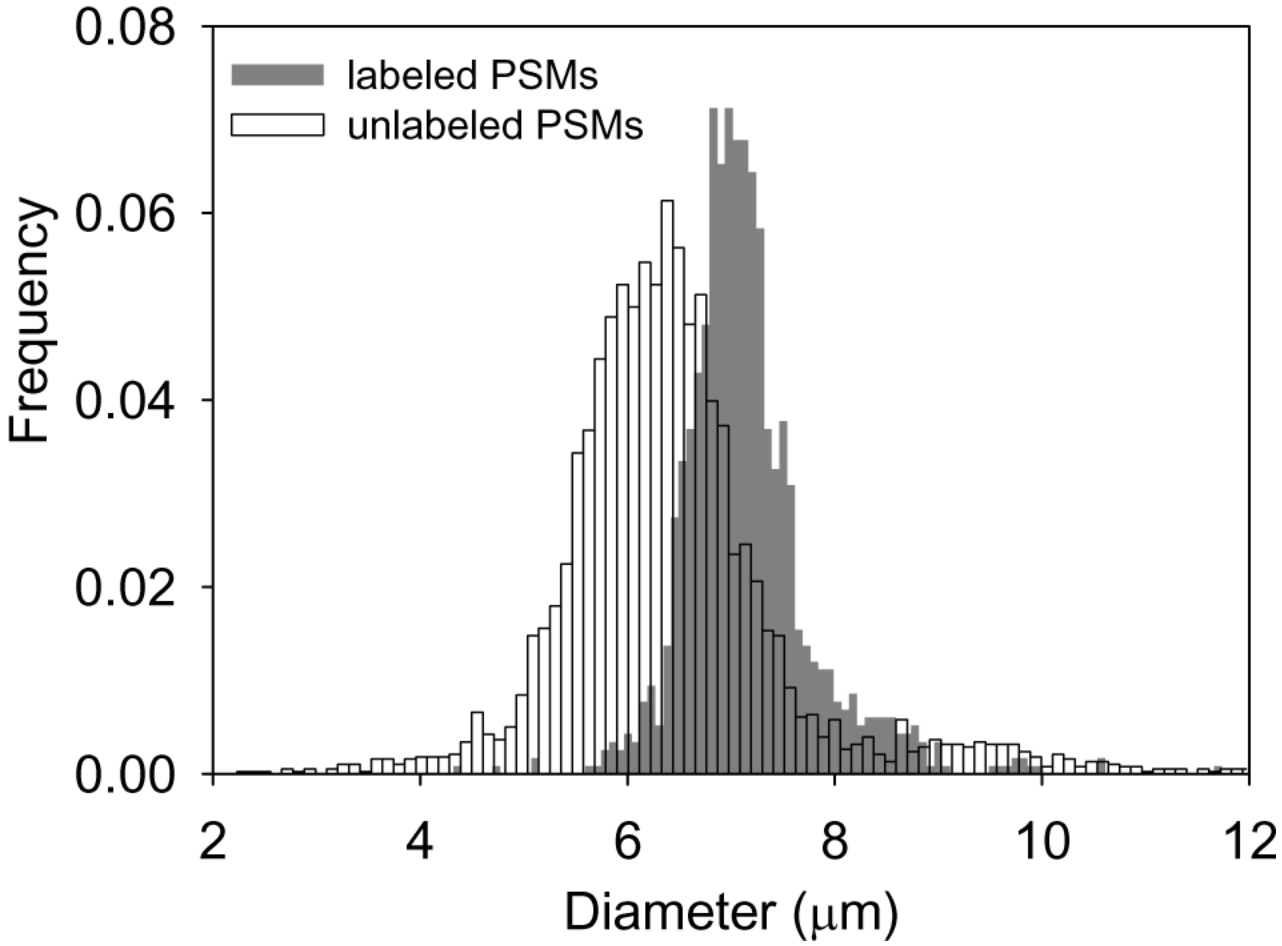

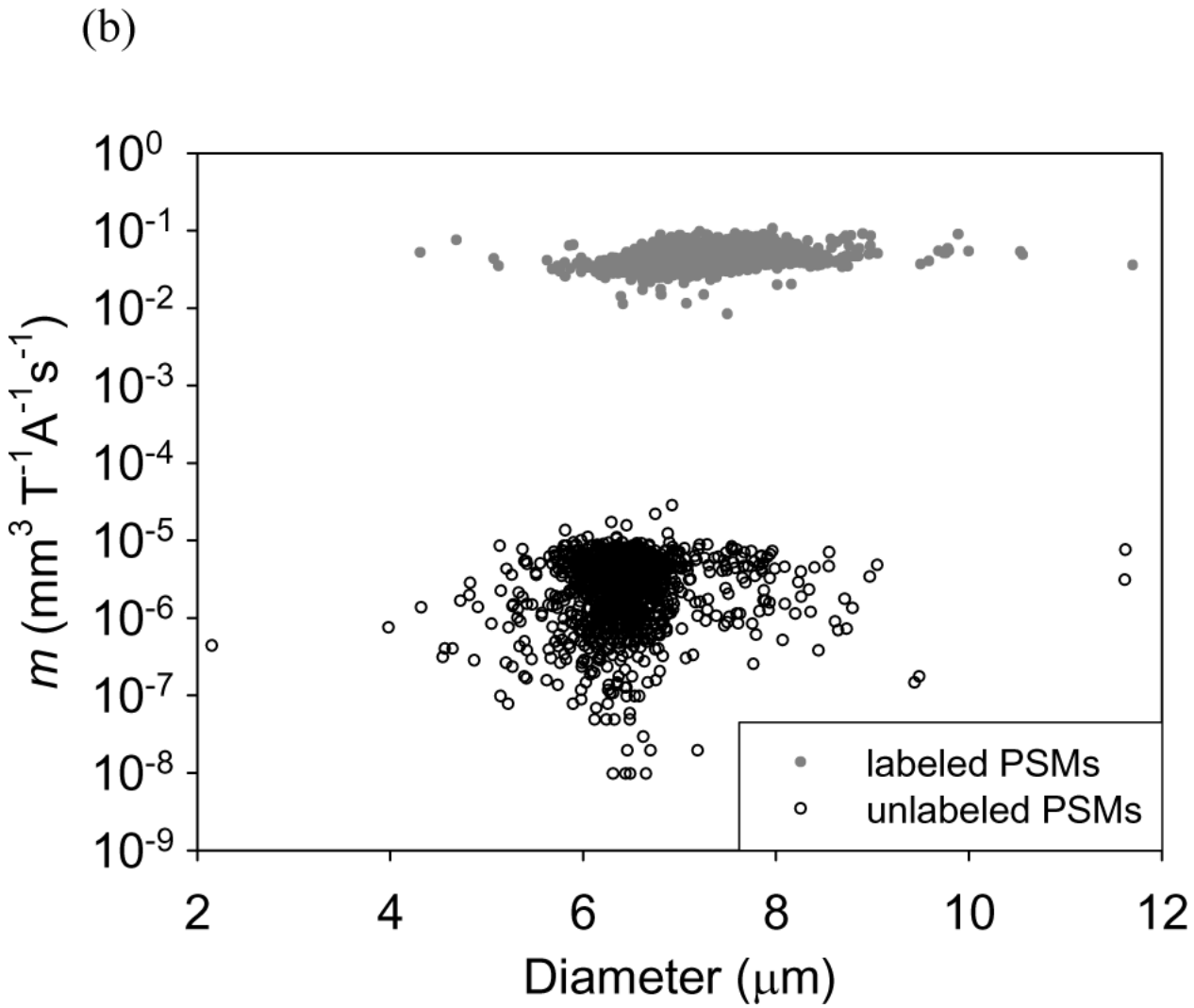

Fig. 5.

A plot of the diameter of unlabeled and labeled PSMs using a density of 1.052 g cm^{-3} for both populations of spheres, (a). The labeled PSMs were labeled with MACS™ anti-biotin nanoparticles. (b) is a dot plot of the MM and diameter of the unlabeled and labeled PSMs presented in (a). Note shift in the PSMs mobility and the apparent diamater upon binding of the magnetic nanoparticles.

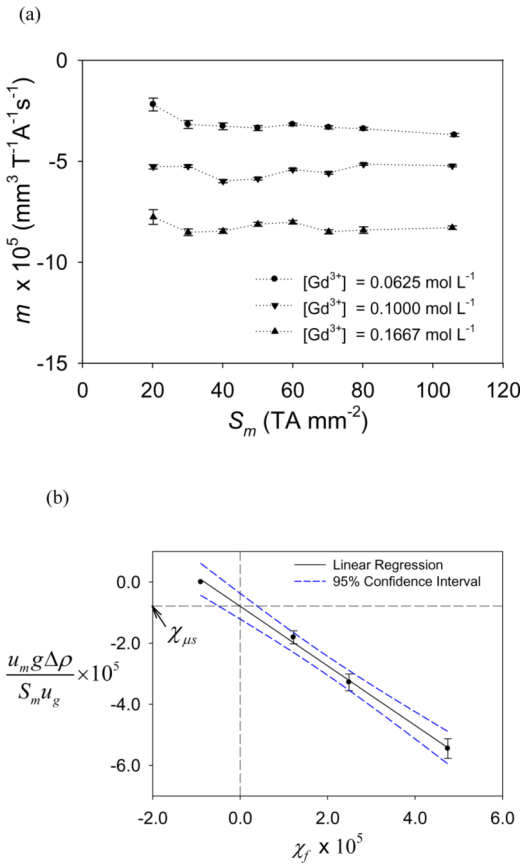

Fig. 6.

(a) MM of unlabeled PSMs as a function of S_m ranging from 10.3 to 106 TA mm^{-2}. The three lines correspond to the three sets of experiments conducted in solutions of different magnetic susceptibility. (b) The ratio of magnetically induced velocity to settling velocity as a function of magnetic susceptibility of the suspending buffer. Note: the error bar represents the 95% confidence interval of the mean value.

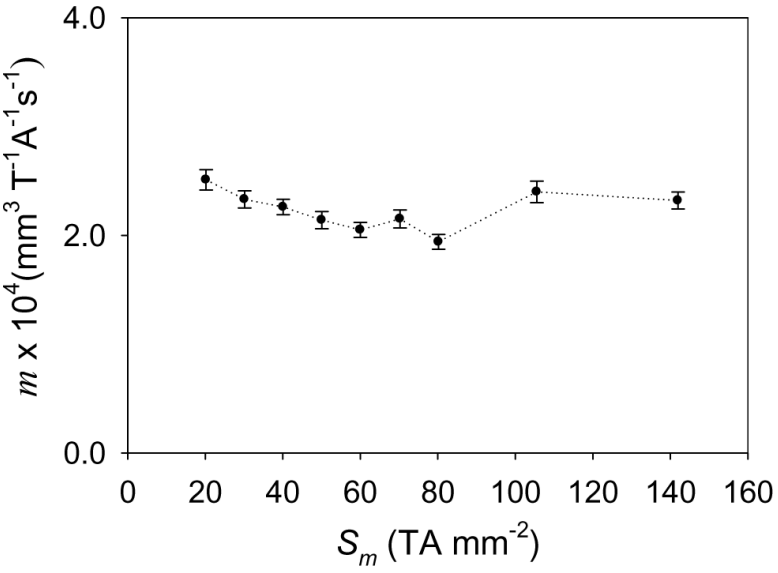

Fig. 7.

MM of the *Bacillus globigii* as a function of S_m ranging from 20.2 to 142 TA mm^{-2}. Note: the error bar represents the 95% confidence interval of the mean value.

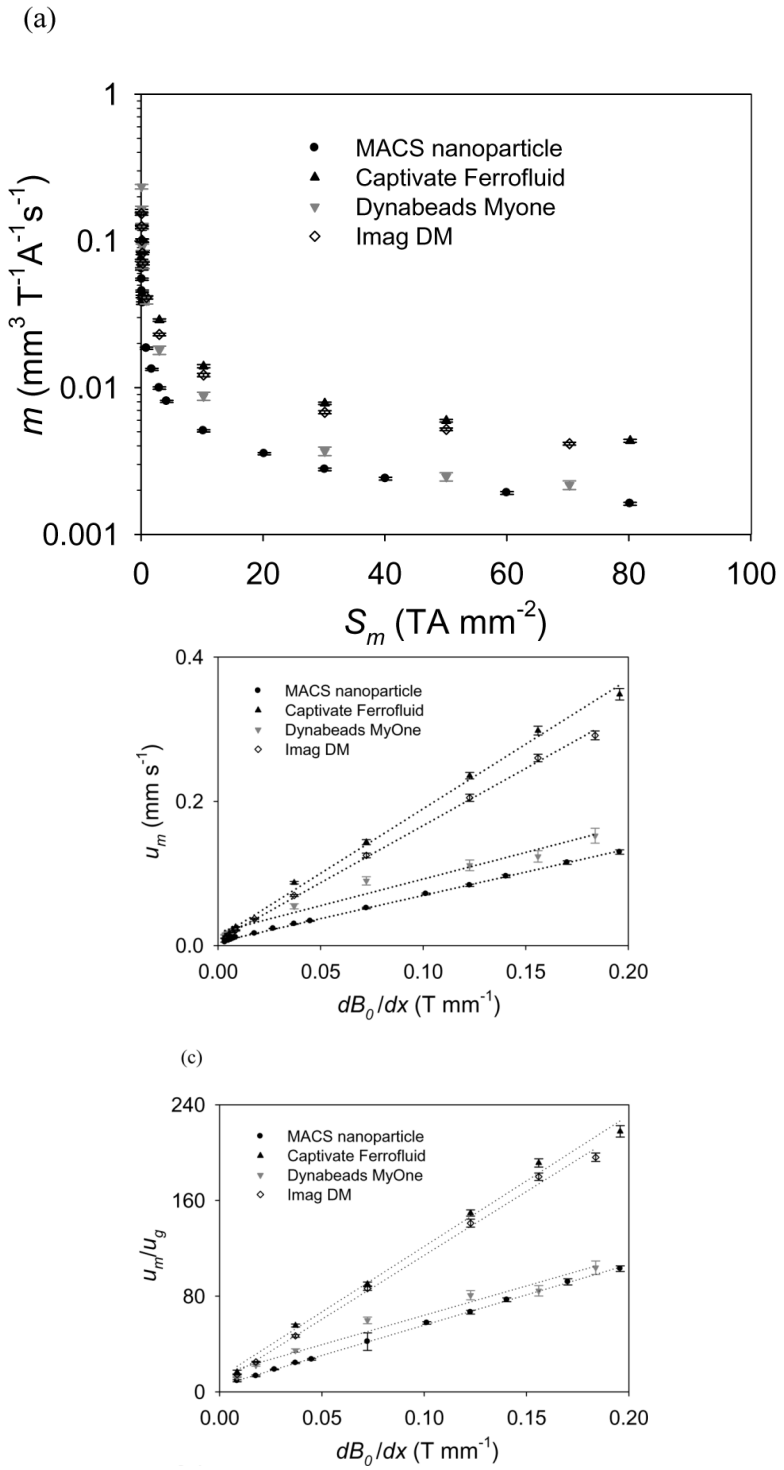

Fig. 8.

(a) MM as a function of S_m for the PSMs labeled with: MACS antibiotin nanoparticles, Cativate Ferrofluid, Dynabeads MyOne, Imag DM particles. (b) The magnetically induced velocity as a function of dB_0/dx. (c) The ratio of the magnetically induced to the settling velocity as a function of dB_0/dx (only data above the saturation point, $dB_0/dx \approx 0.008$ T mm^{-1}). Note: the error bar represents the 95% confidence interval of the mean value.

Table 1

Numeric value of the slope, intercept, R^2 of the data presented in Fig. 8 (c) and calculated saturation magnetization of the labeled PSM complex determined from eqn (13). The abbreviations are explained in the text accompanying eqn (13).

Type of nanoparticle	Slope (mm T^{-1})	Intercept (u_m/u_g)	R^2	$M_{s,ave}$ (A m^{-1})
MACS	507	5.0	0.999	256
Captivate	1,096	11.9	0.994	554
Dynabeads	491	14.9	0.969	248
Imag DM	1,068	7.2	0.997	540

Table 2

Size characteristics of the labeled PSM-nanoparticle complexes and the saturation magnetization of the magnetic nanoparticles. The abbreviations are explained in the text accompanying eqns (4) and (7).

Type of nanoparticle	Calculate D_t (μm)	V_t (m^3)	$N_{ns}V_{ns}$(= V_t - $V_{\mu s}$, m^3)	M_s(A m^{-1})
MACS	7.20	1.95×10^{-16}	3.80×10^{-17}	1,318
Captivate	7.97	2.65×10^{-16}	1.08×10^{-16}	1,365
Dynabeads	8.19	2.88×10^{-16}	1.30×10^{-16}	548
BD Imag	7.78	2.45×10^{-16}	8.91×10^{-17}	1,495